UNIVERSITY OF STOCKHOLM
INSTITUTE OF PHYSICS

REPORT

COHERENT PRODUCTION OF TWO AND THREE PIONS IN pd REACTIONS AT 19 GeV/c

V. Bakken, H. Gennow, P. Lundborg, J. Mäkelä, R. Møllerud, M. Pimiä, B. Selldén, E. Sundell and J.K. Tuominemi

USIP Report 76 - 27 October 1976

COHERENT PRODUCTION OF TWO AND THREE PIONS IN pd REACTIONS AT 19 GeV/c

V. Bakken[o], H. Gennow[+], P. Lundborg[+], J. Mäkelä[x], R. Møllerud[*], M. Pimiä[x], B. Selldén[+], E. Sundell[oo], and J.K. Tuominemi[x].

ABSTRACT

The coherent reactions $pd \to pd\pi^+\pi^-$, $pd \to pd\pi^+\pi^-\pi^o$ and $pd \to nd\pi^+\pi^+\pi^-$ are studied. In the two first reactions strong production of $\Delta^{++}(1236)$ is observed. Production of d^{*o} and d^{*++} is observed in the first and second reactions respectively. The forward slope of the t-distribution of the $p\pi^+\pi^-$ system in the $pd \to pd\pi^+\pi^-$ channel decreases with increasing mass. The 1500 and 1700 MeV enhancements in the $p\pi^+\pi^-$ mass spectrum of this channel are studied. Assuming that the Gribov-Morrison rule holds, we find by analysing the moments of the decay angular distributions that the resonances N(1470), N(1520) and N(1688) are the most likely resonances to be identified with these enhancements. We find evidence against s-channel helicity conservation and some evidence against t-channel helicity conservation. The decay parameters of the $\Delta^{++}(1236)$ in the reaction $pd \to \Delta^{++}\pi^-d$ are in good agreement with the predictions of a one-pion exchange model.

o) Institute of Physics, University of Oslo

*) The Niels Bohr Institute, University of Copenhagen

+) Institute of Physics, University of Stockholm

x) Department of Nuclear Physics, University of Helsinki

oo) Department of Physics, Åbo Akademi

1. INTRODUCTION

In recent years the phenomenon of diffraction dissociation has attracted great interest. This particular reaction mechanism is believed to dominate particle production at very high energy. One difficulty in studying diffraction dissociation at intermediate energy is that other mechanisms contribute significantly and it is therefore often not possible to isolate purely diffractive events. In this paper we will take advantage of the fact that when a system of particles X is produced in a coherent reaction of the type

$$p + d \rightarrow X + d$$

the isospin of the exchange has to be zero. Coherent reactions of this type are therefore suitable for studies of diffractively produced systems.

The following reactions will be studied

$$pd \rightarrow pd\pi^+\pi^- \tag{1a}$$

$$pd \rightarrow pd\pi^+\pi^-\pi^0 \tag{1b}$$

$$pd \rightarrow nd\pi^+\pi^+\pi^- \quad . \tag{1c}$$

The experimental procedures and the channel cross sections have been presented in an earlier paper [1]. The number of events and the channel cross sections are also given in Table 1. For reactions (1b) and (1c) we use only events where the recoil deuteron has been measured. The general features of the reactions are described in Sect. 2. The reaction (1a) will be analysed in more detail in Sects. 3-6. Sect. 3 contains a study of the longitudinal phase space plot. In Sect. 4 the slope of the four-momentum transfer distribution, $d\sigma/dt_{dd}$, will be studied as a function of the mass of the $p\pi^+\pi^-$ system. A moment analysis of the decay angular distributions of the $p\pi^+\pi^-$ system is presented in Sect. 5. The results of this analysis will be compared with earlier studies of $p\pi^+\pi^-$ systems produced in pp and pd reactions. The decay parameters of the $\Delta^{++}(1236)$ are determined in Sect. 6.

2. RESONANCE PRODUCTION

2.1 The $pd \to pd\pi^+\pi^-$ channel

We first investigate the effective mass distributions in reaction (1a). The distribution of the $d\pi^-$ mass, presented in Fig. 1b, shows a strong enhancement at around 2200 MeV. This structure, the so called d^*, is known from other high energy experiments with deuteron targets [2-3]. It is interpreted to be due to an interaction between the outgoing negative pion and one of the nucleons in the deuteron, leading to the formation of a Δ (1236) resonance. This resonance then decays back to a π^- and a nucleon, and the nucleons recombine to form a deuteron [2]. The distribution of the π^- with respect to the direction of the incoming proton in the $d\pi^-$ rest system exhibits a strong peak in the forward direction for the d^* events (not shown). This fact shows that the d^* is not a resonance.

The distribution of the $d\pi^+$ mass, Fig. 1a, shows a much weaker signal at low masses. This can be understood since most of the π^+ come from the Δ^{++} decay and the process, where π^+ is exchanged between the incoming proton and the deuteron, is less probable.

We estimate the cross section for events with the d^{*0} to be (0.09 ± 0.01) mb. In the following, when we study the $p\pi$ and $p\pi^+\pi^-$ mass distributions we exclude events with $M(d\pi^-) < 2.3$ GeV/c, since the d^*-events cannot be considered as truly coherent.

The $p\pi^+$ mass distribution is shown in Fig. 2a. Strong production of $\Delta^{++}(1236)$ is seen. By counting the events above a handdrawn background the Δ^{++} production cross section is estimated to be (150 ± 20) μb. The $p\pi^-$ mass distribution, shown in Fig. 2b, shows only a weak indication of $\Delta^0(1236)$ production.

In Fig. 2c the distribution of the $p\pi^+\pi^-$ mass is shown. Enhancements at 1500 and 1700 MeV are clearly seen. There is also an indication of a structure at 2100 MeV which could be due to the $N(\sim 2100)$. The shaded area in Fig. 2c shows the $\Delta^{++}\pi^-$ mass spectrum. The 1500 and 1700 MeV enhancements are clearly visible also in this distribution. In the low mass region the $p\pi^+$ mass is, however, confined to the Δ-band by kinematics and it is therefore difficult to estimate the branching

ratio for this particular decay mode. In the mass region between 1.6 - 2.0 GeV/c^2 about 50 % of the events are in the Δ-band.

The $\pi^+\pi^-$ mass distribution (not shown) is smooth without any clear indication of ρ or f meson production.

2.2 The pd → pd$\pi^+\pi^-\pi^0$ channel

Strong d^{*++} production is seen in the $d\pi^0$ mass distribution of reaction (1b), Fig. 3c. The amount of genuine d^{*++} production is however difficult to ascertain since influx from multi-neutral channels is likely in this part of the phase space. In the $d\pi^-$ mass distribution some d^{*0} production is seen, Fig. 3b, while the $d\pi^+$ distribution is structureless, Fig. 3a. In the subsequent analysis we exclude those events for which $M(d\pi^0) < 2.22$ GeV.

The $p\pi^+$, $p\pi^-$ and $p\pi^0$ mass distributions are shown in Fig. 4. The Δ(1236) signal is clearly seen in all the three distributions. It is especially strong in the $p\pi^+$ distribution as expected. The $\Delta^{++}(1236)$ cross section is estimated to be (0.07 ± 0.01) mb by counting events above a handdrawn background.

The $p\pi^+\pi^-$, $p\pi^+\pi^0$ and $p\pi^-\pi^0$ mass distributions have been plotted in Fig. 5. The two first distributions appear rather structureless while in the $p\pi^-\pi^0$ distribution N(≈ 1500) and N(≈ 1700) signals are seen. The difference between the $p\pi^-\pi^0$ distribution and the other two distributions might be due to the fact that the $\Delta^{++}(1236)$ production is stronger than the production of $\Delta^+(1236)$ and $\Delta^0(1236)$.

We have also examined the $\pi\pi$ mass distributions and observed clear $\rho^-(770)$ production Fig. 6c, and weaker ρ^+ and ρ^0 production (Fig. 6a-b). In the scatter-plot of $M(p\pi^+)$ vs $M(\pi^-\pi^0)$, not shown, we see an indication of associated $\Delta^{++}\rho^-$ production. The mass distribution of the $p\pi^+\pi^-\pi^0$ system itself does not exhibit any particular structure, Fig. 7a.

Production of ω(784) is possible in this channel and we therefore show the $\pi^+\pi^-\pi^0$ mass distribution in Fig. 6b. The ω signal is clear although not very strong. The cross section for ω production is estimated to (13 ± 4) μb, corrected for the branching ratio. We also see structures at the positions of the φ(1020) and the $A_2(1310)$.

2.3 The $pd \to nd\pi^+\pi^+\pi^-$ channel

We have studied the $d\pi^+$ and $d\pi^-$ mass distributions but we have not found any indication of d^* production.

The $n\pi^+$ and $n\pi^-$ mass distributions are plotted in Fig. 8. The $n\pi^+$ mass distribution is characterized by a broad low mass enhancement. In the $n\pi^-$ mass distribution a strong $\Delta^-(1236)$ signal is observed. The cross section for $\Delta^-(1236)$ production has been estimated to (47 ± 10) μb. Some ρ^o production is seen in the $\pi^+\pi^-$ mass distribution (not shown). The $\pi^+\pi^+\pi^-$ mass distribution is structureless, Fig. 8c.

3. LONGITUDINAL PHASE SPACE ANALYSIS

The technique of longitudinal phase space analysis has been extensively used to analyse high energy reactions. The basic idea is that at high energy most of the available energy is spent on giving large longitudinal momenta to the created particles rather than on creating a large number of particles or giving them large transverse momenta. The interesting dynamical properties of the interaction should then reveal themselves in the structure of the longitudinal momentum distributions. In particular the technique has been used to investigate diffraction dissociation [4].

In accordance with [5] we use the CMS longitudinal momenta, q, of the particles to define

$$Q = \sum_i |q_i| , \qquad x_i = 2q_i/Q .$$

The index i denotes one of the four outgoing particles in reaction (1a), 1 = p, 2 = d, 3 = π^+, 4 = π^-. Since the proton and the deuteron have to go into opposite hemispheres there are only four possible configurations:

$$x_1, x_3, x_4, > 0 > x_2 \tag{2a}$$

$$x_1, x_3 > 0 > x_4, x_2 \tag{2b}$$

$$x_1, x_4 > 0 > x_3, x_2 \tag{2c}$$

$$x_1 > 0 > x_3, x_4, x_2 \tag{2d}$$

In the (x_3, x_4) plane the configurations (2a) and (2d) form triangles while (2b) and (2c) form squares.

In order to divide away the phase space factor each event is given a weight [6]

$$w(x) = (\sum_{i=1}^{n} x_i^2/E_i)(\prod_{i=1}^{n} E_i)(Q/2)^{3-n}$$

where E_i is the CMS energy of the particle i and n is the number of particles. The (x_3, x_4) plane is divided into bins ($\Delta x = 1/8$) and for each bin the total

weight $\sum_{\gamma} w_{\gamma}$ for all events γ in the bin is defined as N_w. The normalized weight for each bin is defined as

$$\Delta_w = \sigma N^{-1} s^{-1} N_w$$

where N is the total number of events σ the channel cross section and s the CMS energy squared.

The LPS plot for reaction (1a) is shown in Fig. 9. As can be seen nearly all events are concentrated to the region $0 < x_3, x_4 < 3/8$. The upper triangular region is very similar to the corresponding one for the channel $pp \to pp\pi^+\pi^-$ at 19 GeV/c [4a] but the cross sections are about three times smaller for the coherent channel in the region $1/8 < x_3, x_4 < 3/8$. The shape with a broad enhancement is characteristic for diffraction dissociation which thus seems to dominate the production process in that part of the longitudinal phase space.

4. THE t DISTRIBUTIONS OF THE $p\pi^+\pi^-$ SYSTEM

The t distributions of the $p\pi^+\pi^-$ system are shown in Fig. 10 for three different mass intervals. We have fitted exponentials of the form Ae^{bt} to the distributions and obtained the values of A and b that can be found in Table 2. According to [7] the slope of the t distribution of the coherent reaction $pd \rightarrow pd\pi^+\pi^-$ is related to the slope of the t distribution of the corresponding non-coherent reaction $pp \rightarrow pp\pi^+\pi^-$ in the same t interval by the relation

$$|\text{coherent slope}| \approx |\text{hydrogen slope}| + 1/2\,\alpha$$

where $\alpha = 32.7\ (\text{GeV/c})^{-2}$.

We have therefore plotted the slopes found for the coherent distribution together with the corresponding slopes obtained from fits to the t distributions of our $pp \rightarrow pp\pi^+\pi^-$ events [8]. We have added $1/2\ \alpha = 16.4$ to the non-coherent slopes. As can be seen the overall agreement is good. In both cases the slope decreases when the mass increases.

5. THE DECAY ANGULAR DISTRIBUTIONS OF THE $p\pi^+\pi^-$ SYSTEM

The $p\pi^+\pi^-$ mass distribution of Fig. 2c shows enhancements at 1470 MeV and at 1700 MeV. The 1470 MeV enhancement has been observed in the reaction $pd \to pd\pi^+\pi^-$ at 7 and 11.6 GeV/c [9,10] while the 1700 MeV enhancement was rather weak at these energies. Both structures have been observed in the reaction $pp \to pp\pi^+\pi^-$ at 12, 19 and 24 GeV/c [8,11]. Since the $p\pi^+\pi^-$ system in the reaction (1a) has to be in an isospin 1/2 state while it in the pp case can be in an either I = 1/2 or I = 3/2 state, it is of great interest to compare the decay angular distributions of the coherently and non-coherently produced $p\pi^+\pi^-$-systems with one another. From such a comparison it might be possible to identify these enhancements with known isobars.

The decay angular distributions have been investigated in the Gottfried-Jackson or t-channel helicity frame and in the s-channel helicity frame. In the t-channel frame the z-axis is defined by the direction of the incoming proton whereas in the s-channel frame it is defined by the direction of the $p\pi^+\pi^-$ system in the CM system. The y-axis is the same in both frames, namely the normal of the production plane (see also Fig. 11).

The normal of the decay plane, defined by $\vec{p}_p \times \vec{p}_{\pi^+}$, gives two angles in the t-channel frame β and ϕ_{TY} (the Treiman-Yang angle), see Fig. 11a. Since there are some indications of a sequential decay, i.e. $N^* \to \Delta^{++}\pi^-$, we will also study the distributions of the angles of the direction of the Δ^{++} in the t-channel frame, ϑ and ψ_{TY}, Fig. 11b. The azimuthal angle ψ_H of the direction of the Δ^{++} will be used to test s-channel helicity conservation, Fig. 11c.

The intensity as a function of β and ϕ_{TY} can be expanded in terms of spherical harmonics $Y_\ell^m(\cos\beta, \phi_{TY})$

$$W(\beta,\phi) = \sum_{m,m'} \rho_{m,m'} \sum_{M\ell}\sum C(J,J,\ell;\, m',\, -m)C(J,J,\ell;\, M,\, -M)$$

$$(-1)^{M-m} \sqrt{\frac{4\pi}{2\ell+1}}\, Y_\ell^{m-m'}(\cos\beta,\, \phi_{TY}) |R_M|^2 \quad .$$

Here J is the spin of the $p\pi^+\pi^-$ system, $\rho_{mm'}$ are the density matrix elements and R_M the decay amplitudes [12]. M is the spin projection on the direction of analysis in this case along the normal of the decay plane.

The four lowest moments $\langle Y_L^0(\cos\beta)\rangle$ are shown in Fig. 12 as a function of the mass of the $p\pi\pi$ system. For comparison we also show the same moments for the reaction $pp \to pp\pi^+\pi^-$. The number of events in each mass bin is given in Table 3. No d^* cut has been applied. The moments for $L > 5$ (not shown) are consistent with being zero.

We notice from Fig. 12 that the moments for odd L are all consistent with being zero. The distributions of $\langle Y_2^0\rangle$ are rather similar in the two cases. In the 1400-1500 MeV region, which corresponds to the first enhancement, $\langle Y_2^0\rangle$ is different from zero by 3 standard deviations in the coherent reaction and by 2 standard deviations in the non-coherent reaction [8], which implies $J \geq 3/2$.

In the 1660-1770 MeV region, which corresponds to the second enhancement, $\langle Y_2^0\rangle$ is clearly different from zero in both cases. In the coherent case $\langle Y_4^0\rangle$ is different from zero by 3.5 standard deviations. In the non-coherent case it begins to rise significantly only above 1.77 GeV.

In order to gain more information on the angular momentum of the $p\pi^+\pi^-$ system we now turn to the distributions of θ, the direction of the Δ^{++}. We then use only those events for which $1.15 < M(p\pi^+) < 1.30$ GeV.

The moments $\langle Y_L^0(\cos\theta)\rangle$ have been plotted in Fig. 13 both for the coherently and for the non-coherently produced $p\pi\pi$ systems. We note that $\langle Y_1^0\rangle$ is different from zero over the whole mass range which implies interference between waves of different parity. In the 1400-1500 MeV region the higher moments are compatible with being zero in both cases, which implies that $J \geq 1/2$. In the 1660-1770 MeV region $\langle Y_2^0\rangle$ is in both cases large which implies the presence of at least spin 3/2. In the coherent case $\langle Y_4^0\rangle$ is again somewhat different from zero (3 standard deviations). This indicates the $J = 5/2$ spin component is stronger in the coherent case than in the non-coherent case in the 1700 MeV region.

We will now compare our results with those found in earlier studies of these enhancements. Hochman et al. [10] studied the 1400-1500 MeV enhancement and found that the spin is either 1/2 or 3/2, which is in agreement with our results. Blobel et al. [11] in their partial wave analysis found that the $\frac{3^-}{2}$ amplitude is dominant but the $\frac{1^+}{2}$ amplitude is also present in the 1400-1500 MeV region. In the 1700 MeV region they again found the $\frac{3^-}{2}$ amplitude dominant but the $\frac{1^+}{2}$ and $\frac{5^+}{2}$ contributions are not negligible. Our results are thus consistent with what they have found.

It is tempting to try to identify the two enhancements with known isobars. If we assume that they are purely diffractively produced in the coherent case and that the Gribov-Morrison rule [13] holds, we have the following possible candidates: N(1470) $J^P = \frac{1^+}{2}$ (the Roper resonance), N(1520) $J^P = \frac{3^-}{2}$, and N(1688) $J^P = \frac{5^+}{2}$. In the non-coherent case we cannot exclude other exchanges and we then have several additional candidates: N(1670) $J^P = \frac{5^-}{2}$, N(1700) $J^P = \frac{1^-}{2}$, Δ(1650) $J^P = \frac{1^-}{2}$ and Δ(1670) $J^P = \frac{3^-}{2}$.

From the values of the moments we conclude that it is likely that both N(1470) and N(1520) contribute to the 1400-1500 enhancement in both the coherent and in the non-coherent case. For the 1700 enhancement the N(1688) is the only possible candidate. The fact that $\langle Y_4^0 \rangle$ is different from zero supports this conclusion further. In the non-coherent case the Δ(1670) is maybe also present which would explain the absence of a non-zero $\langle Y_4^0 \rangle$ moment. It must be kept in mind however that the resonance nature of these two enhancements is far from being settled [11].

The question of t-channel and s-channel helicity conservation (TCHC, SCHC) [14] in diffractive processes has been extensivly discussed during the last years [2, 8, 10, 11]. A necessary condition for the helicity to be conserved is isotropy of the corresponding azimuthal angular distribution or, equivalently the vanishing of all moments $\langle Y_l^m \rangle$ with $m \neq 0$. We have calculated three such moments and used both the direction of the proton and the direction of the Δ^{++}

as analyzers. As can be seen in Fig. 14 TCHC seems to hold when the analyzer is the direction of the proton. This is in agreement with the results of [10] but not in agreement with [2]. SCHC seems not to hold in agreement with both [2] and [10].

If we use the direction of the Δ^{++} as an analyzer, Fig. 15, neither TCHC nor SCHC seems to hold in agreement with earlier results [2, 8].

To investigate the question of helicity conservation further we have plotted the azimuthal angles of the Δ^{++} and the proton both in the t-channel and s-channel helicity frames in Fig. 16a-d for all events. The distributions in the t-channel helicity frame seem to be rather flat. From the corresponding moments we find that the χ^2 - probability for helicity conservation is 12 % if the proton is used as analyzer and 2 % if the Δ^{++} is used as analyzer. The distributions in the s-channel helicity frame are less isotropic and the values of the moments show that the s-channel helicity is not conserved.

6. DECAY ANGULAR DISTRIBUTIONS OF THE Δ^{++}

The decay angular distributions $\cos\theta$ and ϕ in the t-channel helicity frame for the Δ^{++} in the reaction $pd \rightarrow \Delta^{++}\pi^{-}d$ are shown in Fig. 16 e-f. The density matrix elements were evaluated from the moments of the distributions and the result is given in table 4, where we also compare our results with those obtained in other experiments, and with theoretical predictions. The agreement between our results and the predictions of the one-pion exchange model (OPE) is good. Our results do not agree with the predictions of the Stodolsky-Sakurai model [17] for vector-meson exchange. We thus conclude that one-pion exchange is the most likely mechanism for the reaction $pd \rightarrow \Delta^{++}\pi^{-}d$.

ACKNOWLEDGEMENTS

We wish to thank the staffs of the CERN Proton Synchrotron, of the 2m hydrogen bubble chamber and of the U5 beam for their efforts during the exposures for this experiment.

Our thanks are also due to the scanning and measuring staffs at our four universities and the staffs of the computing centers in Copenhagen, Helsinki, Oslo and Stockholm.

Supports from Research Councils in Denmark, Finland, Norway and Sweden are gratefully acknowledged.

REFERENCES

1 V. Bakken, H. Gennow, T. Jacobsen, P. Lundborg, R. Möllerud, J. Mäkelä, J. Olsson, M. Pimiä, B. Selldén, G. Skjevling and E. Sundell, One, two and three pion production in pd collisions at 19 GeV/c, to be published.

2 J.W. Chapman, J.W. Cooper, B.P. Roe, D. Sinclair and J.C. Van der Velde, Phys. Rev. Lett. 30 (1973) 64.

3 M.A. Abolins, D.D. Carmony, R.L. Lander and Ng.-h Xuong, Phys. Rev. Lett. 15 (1965) 125

G. Vegni, H. Winzeler, P. Zaniol, P. Fleury and Y. De Rosny, Phys. Lett. 19 (1965) 526

H. Braun, D. Evrard, A. Fridman, J.P. Gerber, A. Givernaud, R. Kahn, G. Maurer, A. Michalon, B. Schiby, R. Strub and C. Voltolini, Phys. Rev. D3 (1971) 2572

M. Month, Phys. Rev. 155 (1967) 1689

D. Evrard, A. Fridman and A.C. Hirschfeld, Nucl. Phys. B14 (1969) 699

R. Vanderhagen, G. De Rosny, N. Armenise, B. Ghidini, A. Romano, A. Forino, M. Goldberg, Nucl. Phys. B13 (1969) 329

W.J. Podolsky, Bull. Am. Phys. Soc. 19 (1974) 568

B.S. Neganov, L.B. Parfenov, J. Exptl. Theoret. Phys. 34 (1957) 767

E.G. Pewitt, T.H. Fields, G.B. Yodh, J.G. Fetkovich and M. Derrick, Phys. Rev. 131 (1963) 1826

F. Turkot, G.B. Collins and T. Fujii, Phys. Rev. Lett. 11 (1963) 474

J. Banaigs, J. Berger, L. Goldzahl, T. Risser, L. Vu-Hai, M. Cotterau and C. le Brun, Nucl. Phys. B67 (1973) 2

J.C. Anjos, D. Levy and A. Santoro, Nucl. Phys. B67 (1973) 37

I. Bar-Nir, T. Risser and M.D. Shuster, Nucl. Phys. B87 (1975) 109.

4a N.K. Yamdagni and S. Ljung, Phys. Letters 37B (1971) 117.

4b W. Kittel, S. Ratti and L. Van Hove, Nucl. Phys. B30 (1971) 333.

5 L. Van Hove, Phys. Letters 28B (1969) 429.

L. Van Hove, Nucl. Phys. B9 (1969) 331.

6 L. Van Hove, Phys. Rep. Phys. Letters 1C (1971) 347.

7 R.S. Panvini, J. Hanlon, W.H. Sims, J.W. Waters, and T.W. Morris, Nucl. Phys. B39 (1972) 538.

8 H. Johnstad, R. Møllerud, L. Veje, S. Ljung, H.I. Miettinen, R.O. Raitio, J.K. Tuominiemi, T. Jacobsen, S.O. Sørensen, L. Granström, S.O. Holmgren, U. Svedin and N. Yamdagni, Nucl. Phys. B42 (1972) 558.

9 U. Karshon, G. Yekutieli, D. Yaffe, A. Shapira, E.E. Ronat, and Y. Eisenberg, Nucl. Phys. B37 (1972) 371.

10 D. Hochman, Y. Eisenberg, U. Karshon, A. Shapira, E.E. Ronat, D. Yaffe, and G. Yekutieli, Nucl. Phys. B68 (1974) 301.

11 V. Blobel, A. Eskreys, H. Fesefeldt, H. Franz, U. Idschok, A. Kotanski, D. Lüers, B. Schröder, N. Schmitz and F. Wagner, Nucl. Phys. B97 (1975) 201.

12 S.M. Berman and M. Jacob, Phys. Rev. 139 (1965) B1023.

13 V.N. Gribov, Yad. Fiz. 5 (1967) 197,
D.R.O. Morrison, Phys. Rev. 165 (1968) 1699.

14 F. Gilman, J. Pumplin, A. Schwimmer and L. Stodolsky, Phys. Lett. 31B (1970) 387.
G. Cohen-Tannoudji, J.M. Drouffe, P. Moussa and R. Peschanski, Phys. Lett. 33B (1970) 183.

15 H. Braun, D. Evrard, A. Fridman, J.-P. Gerber, G. Maurer, A. Michalon, B. Schiby, R. Strub, C. Voltoni, Phys. Rev. D2 (1970) 1212.

16 D. Antich, A. Callahan, R. Carson, C.-Y. Chien, B. Cox, D. Denegri, L. Ettlinger, D. Feiock, G. Goodman, J. Haynes, R. Mercer, A. Pevsner, L. Resvanis, R. Sekulin, V. Sreedhar, R. Zdanis, Nucl. Phys. B29 (1971) 327.

17 L. Stodolsky and J. Sakurai, Phys. Rev. Letters 11 (1963) 90.

FIGURE CAPTIONS

Fig. 1 The $d\pi^+$ (a) and $d\pi^-$ (b) effective mass distributions for the reaction $pd \to pd\pi^+\pi^-$.

Fig. 2 The $p\pi^+$ (a), $p\pi^-$ (b) and $p\pi^+\pi^-$ (c) effective mass distributions for the reaction $pd \to pd\pi^+\pi^-$. The shaded area of (c) shows the $M(\Delta^{++}\pi^-)$ distribution.

Fig. 3 The $d\pi^+$ (a), $d\pi^-$ (b) and $d\pi^0$ (c) effective mass distributions for the reaction $pd \to pd\pi^+\pi^-\pi^0$.

Fig. 4 The $p\pi^+$ (a), $p\pi^-$ (b) and $p\pi^0$ (c) effective mass distributions for the reaction $pd \to pd\pi^+\pi^-\pi^0$.

Fig. 5 The $p\pi^+\pi^-$ (a), $p\pi^+\pi^0$ (b) and $p\pi^-\pi^0$ (c) effective mass distributions for the reaction $pd \to pd\pi^+\pi^-\pi^0$.

Fig. 6 The $\pi^+\pi^0$ (a), $\pi^+\pi^-$ (b) and $\pi^-\pi^0$ (c) effective mass distributions for the reaction $pd \to pd\pi^+\pi^-\pi^0$.

Fig. 7 The $p\pi^+\pi^-\pi^0$ (a) and $\pi^+\pi^-\pi^0$ (b) effective mass distributions for the reaction $pd \to pd\pi^+\pi^-\pi^0$.

Fig. 8 The $n\pi^+$ (a), $n\pi^-$ (b) and $n\pi^+\pi^+\pi^-$ (c) effective mass distributions for the reaction $pd \to nd\pi^+\pi^+\pi^-$.
There are two entries per event in (a).

Fig. 9 Weighted distribution in longitudinal phase space for the reaction $pd \to pd\pi^+\pi^-$.

Fig. 10 The t_{dd} distributions for the reaction $pd \to pd\pi^+\pi^-$,
(a) for $1.3<M(p\pi^+\pi^-)<1.6$ GeV, (b) for $1.6<M(p\pi^+\pi^-)<2.1$ GeV,
(c) for $M(p\pi^+\pi^-)>2.1$ GeV, (d) the fitted slopes as function of the $M(p\pi^-\pi^-)$ mass for the reactions $pd \to pd\pi^+\pi^-$ and $pp \to pp\pi^+\pi^-$.

Fig. 11 Reference frames used in the analysis of Sect. 5.
(a) the normal of the decay plane in the t-channel helicity frame.
(b) and (c) the direction of the Δ in the t- and s-channel helicity frames respectively. $\vec{p}$ and $\vec{p}^{\,*}$ refer to three momentum vectors in the $p\pi^+\pi^-$ rest system and the CM system respectively.

Fig. 12 Moments $\langle Y_\ell^0(\cos\beta)\rangle$ of the angular distributions of the $p\pi^+\pi^-$ decay plane normal in the t-channel helicity frame as functions of the $p\pi^+\pi^-$ mass in the reactions $pd \to pd\pi^+\pi^-$ and $pp \to pp\pi^+\pi^-$.

Fig. 13 Moments $\langle Y_\ell^0(\cos\theta)\rangle$ of the angular distributions of the Δ^{++} direction in the t-channel helicity frame as functions of the $\Delta^{++}\pi^-$ mass in the reactions $pd \to pd\pi^+\pi^-$ and $pp \to pp\pi^+\pi^-$.

Fig. 14 Moments $\langle Y_\ell^m(\cos\theta, \psi)\rangle$ of the angular distributions of the proton in the t-channel and s-channel helicity frames as functions of the $M(p\pi^+\pi^-)$ mass in the reaction $pd \to pd\pi^+\pi^-$.

Fig. 15 Moments $\langle Y_\ell^m(\cos\theta, \psi)\rangle$ of the angular distributions of the Δ^{++} in the t-channel and s-channel helicity frames as functions of the $M(\Delta^{++}\pi^-)$ mass in the reaction $pd \to pd\pi^+\pi^-$.

Fig. 16 Azimuthal angle distributions of the Δ^{++} in the t-channel helicity frame (a), in the s-channel helicity frame (b), of the proton in the t-channel helicity frame (c), in the s-channel helicity frame (d). Angular distributions of the proton in the decay $\Delta^{++} \to p\pi^+$ in the t-channel helicity frame, (e) the polar angle, (f) the azimuthal angle.

TABLE 1. Channel cross sections.

Channel	Events	σ (mb)
$pd \rightarrow pd\pi^+\pi^-$	1016	0.41 ± 0.03
no d*	809	0.35 ± 0.03
$pd \rightarrow pd\pi^+\pi^-\pi^0$	725	0.36 ± 0.04
no d*	461	0.26 ± 0.03
$pd \rightarrow nd\pi^+\pi^+\pi^-$	314	0.15 ± 0.02

TABLE 2. Fits of Ae^{bt} to the t distributions of the $p\pi^+\pi^-$ system.

Mass interval (GeV)	t interval	A (μb)	b $(GeV/c)^{-2}$
1.30 - 1.60	0.02 - 0.16	49 ± 9	37 ± 3
1.60 - 2.10	0.02 - 0.15	43 ± 6	25 ± 2
2.10 -	0.02 - 0.23	37 ± 5	16 ± 2

TABLE 3. Mass bins and numbers of events used for moment analysis.

Mass interval GeV	No of events $p\pi^+\pi^-d$	No of events $\Delta^{++}\pi^-d$	No of events $(p\pi^+\pi^-)p$	No of events $(\Delta^{++}\pi^-)p$
1.40 - 1.51	126	109	308	269
1.51 - 1.58	73	57	225	171
1.58 - 1.66	64	39	216	132
1.66 - 1.77	129	74	372	205
1.77 - 2.00	151	69	511	237

TABLE 4. Δ density matrix elements.

	This exp. $pd \to \Delta^{++}\pi^- d$ 19 GeV/c	[9] $pd \to \Delta^{++}\pi^- d$ 7 GeV/c	[15] $\bar{p}d \to \overline{\Delta^{++}}\pi^+ d$ 5.5 GeV/c	[16] $\bar{p}d \to \overline{\Delta^{++}}\pi^+ d$ 7 GeV/c	OPE	[17] Stodolsky-Sakurai predictions
ρ_{33}	0.05 ± 0.03	0.13 ± 0.04	0.12 ± 0.04	0.04 ± 0.05	0.0	0.375
ρ_{31}	0.00 ± 0.03	0.02 ± 0.03	0.03 ± 0.04	0.10 ± 0.05	0.0	0.216
ρ_{3-1}	-0.01 ± 0.02	0.00 ± 0.03	-0.03 ± 0.04	-0.11 ± 0.05	0.0	0.0

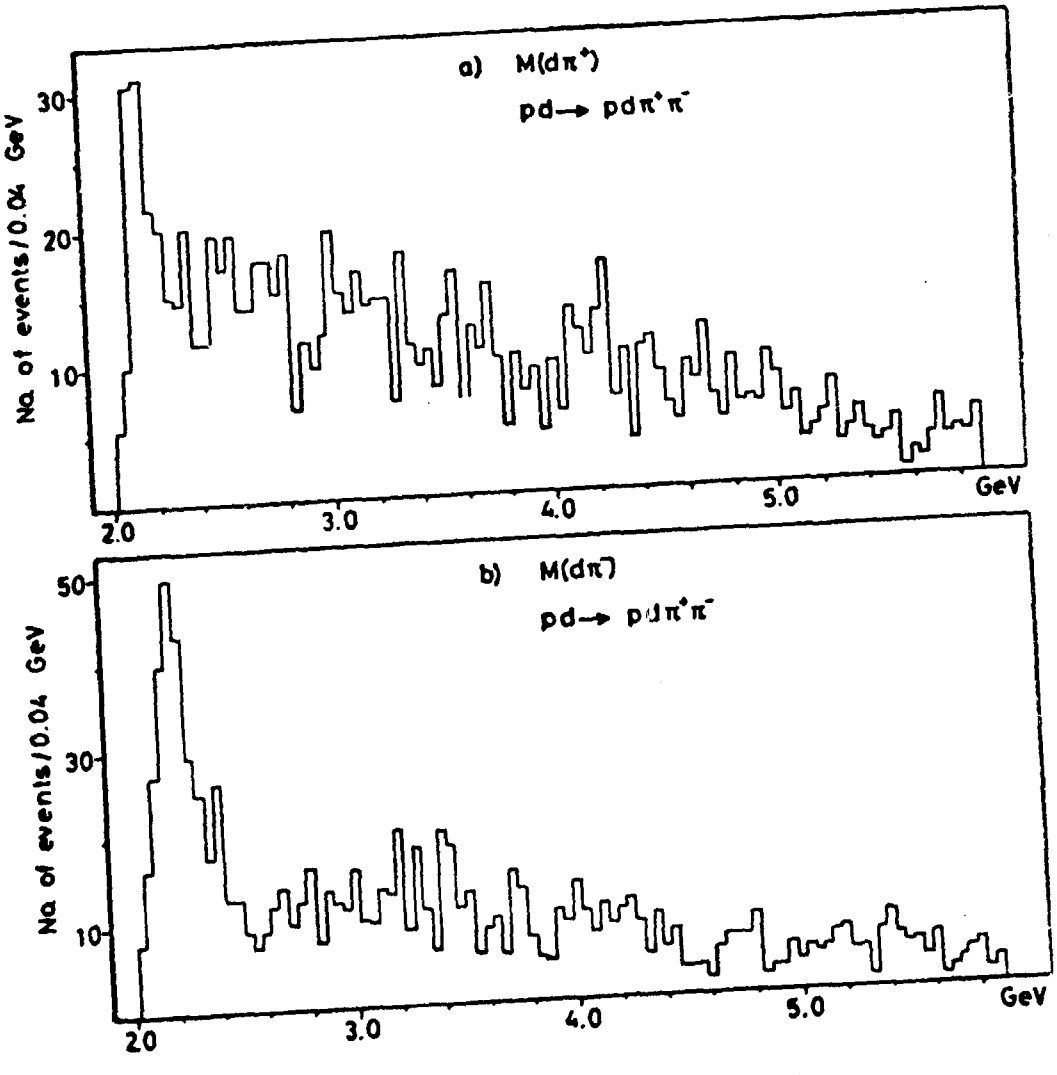
a) M(dπ⁺)
pd→ pdπ⁺π⁻
No. of events/0.04 GeV
30
20
10
2.0
3.0
4.0
5.0
GeV
b) M(dπ⁻)
pd→ pdπ⁺π⁻
No. of events/0.04 GeV
50
30
10
2.0
3.0
4.0
5.0
GeV

Fig. 1

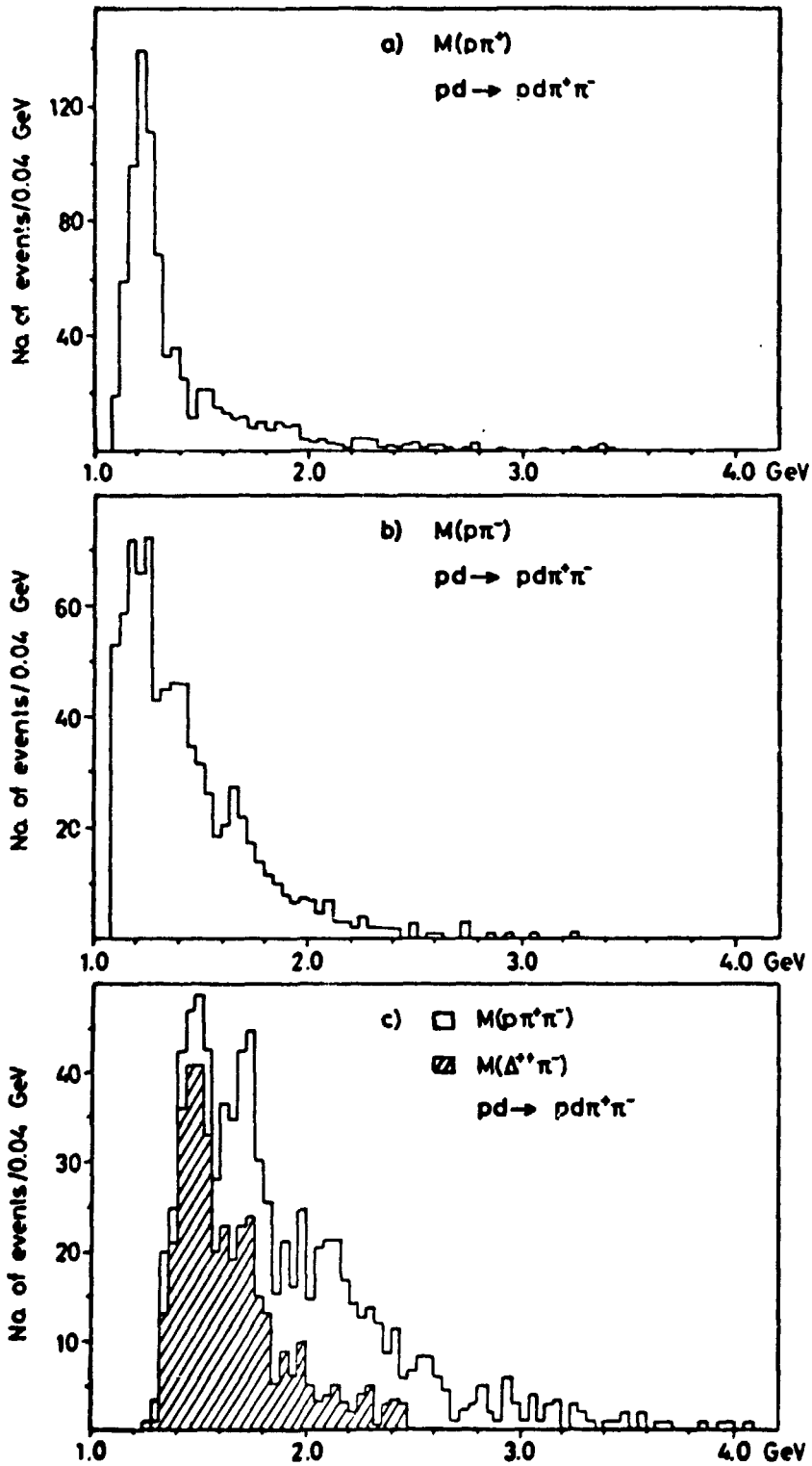
a) M(pπ⁺)
pd→ pdπ⁺π⁻
No of events/0.04 GeV
120
80
40
1.0
2.0
3.0
4.0 GeV
b) M(pπ⁻)
pd→ pdπ⁺π⁻
No of events/0.04 GeV
60
40
20
1.0
2.0
3.0
4.0 GeV
c) M(pπ⁺π⁻)
M(Δ⁺⁺π⁻)
pd→ pdπ⁺π⁻
No of events/0.04 GeV
40
30
20
10
1.0
2.0
3.0
4.0 GeV

Fig. 2

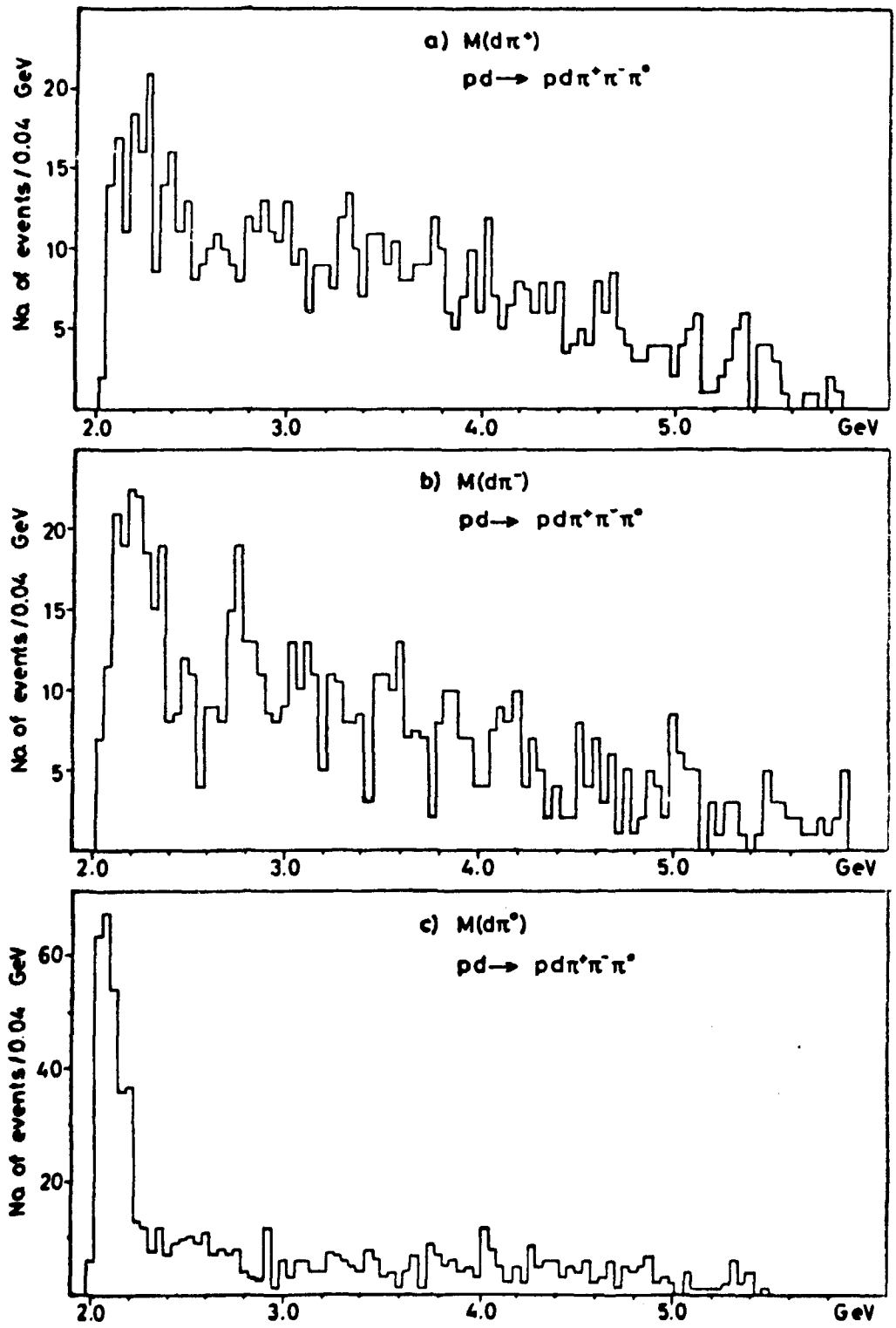
a) M(dπ⁺)
pd→ pdπ⁺π⁻π°
No of events/0.04 GeV
20
15
10
5
2.0
3.0
4.0
5.0
GeV
b) M(dπ⁻)
pd→ pdπ⁺π⁻π°
No of events/0.04 GeV
20
15
10
5
2.0
3.0
4.0
5.0
GeV
c) M(dπ°)
pd→ pdπ⁺π⁻π°
No of events/0.04 GeV
60
40
20
2.0
3.0
4.0
5.0
GeV

Fig. 3

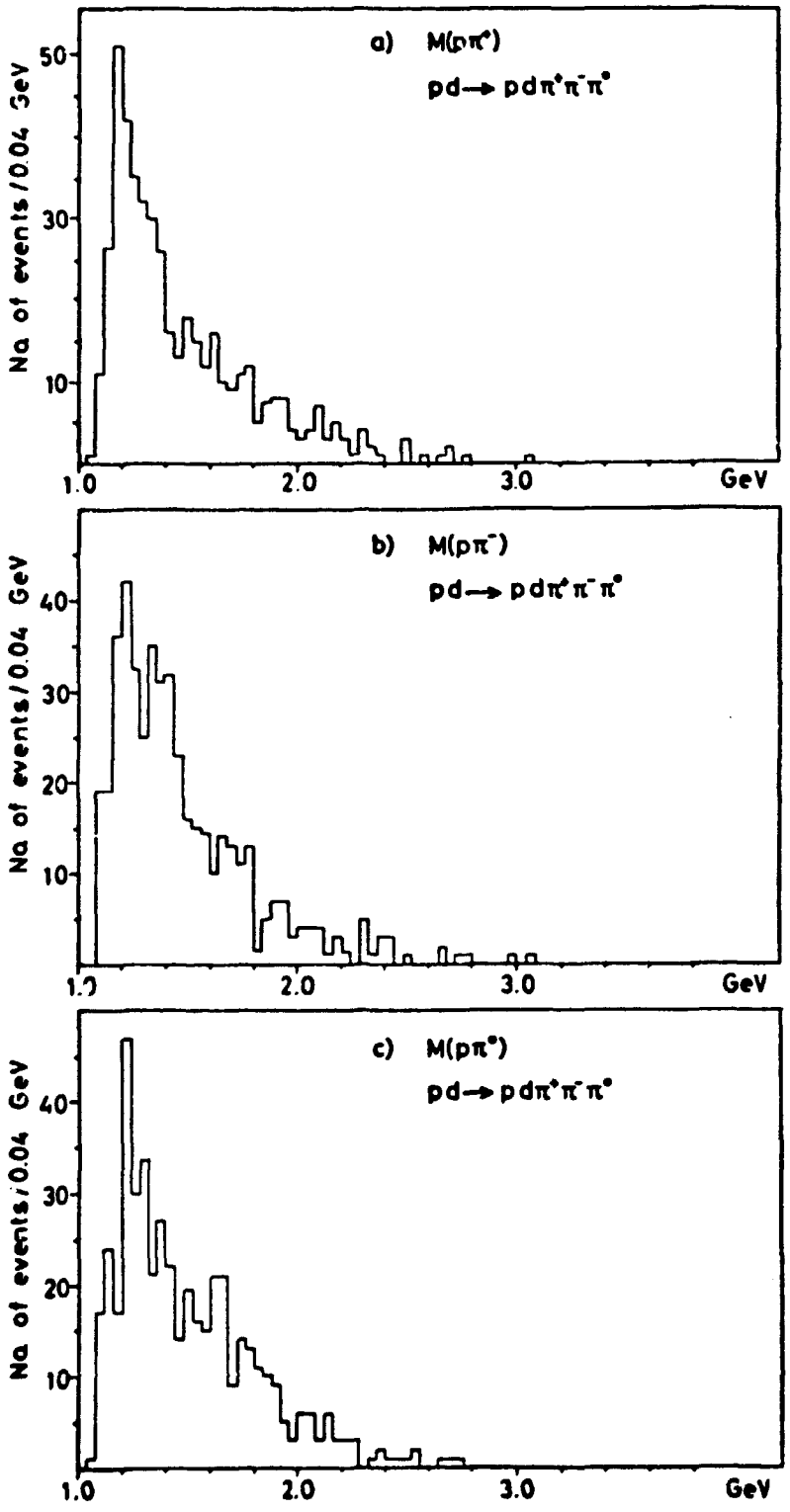
a) M(pπ°)
pd→ pdπ°π⁻π°
No of events/0.04 GeV
50
30
10
1.0
2.0
3.0
GeV
b) M(pπ⁻)
pd→ pdπ°π⁻π°
No of events/0.04 GeV
40
30
20
10
2.0
3.0
GeV
c) M(pπ°)
pd→ pdπ°π⁻π°
No of events/0.04 GeV
40
30
20
10
1.0
2.0
3.0
GeV

Fig. 4

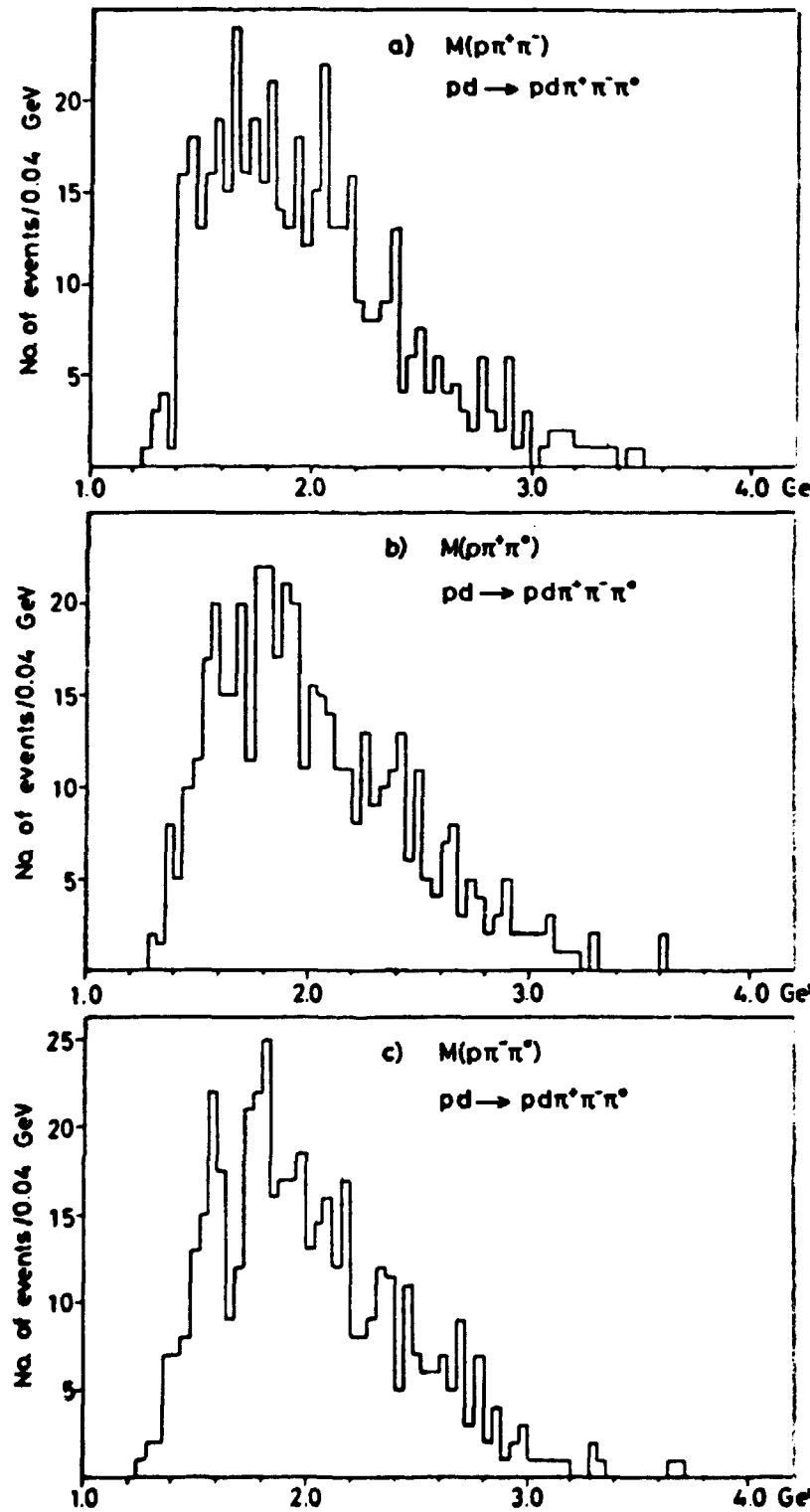
a) M(pπ⁺π⁻)
pd → pdπ⁺π⁻π°
No. of events/0.04 GeV
b) M(pπ⁺π°)
pd → pdπ⁺π⁻π°
No. of events/0.04 GeV
c) M(pπ⁻π°)
pd → pdπ⁺π⁻π°
No. of events/0.04 GeV
1.0
2.0
3.0
4.0 GeV

Fig. 5

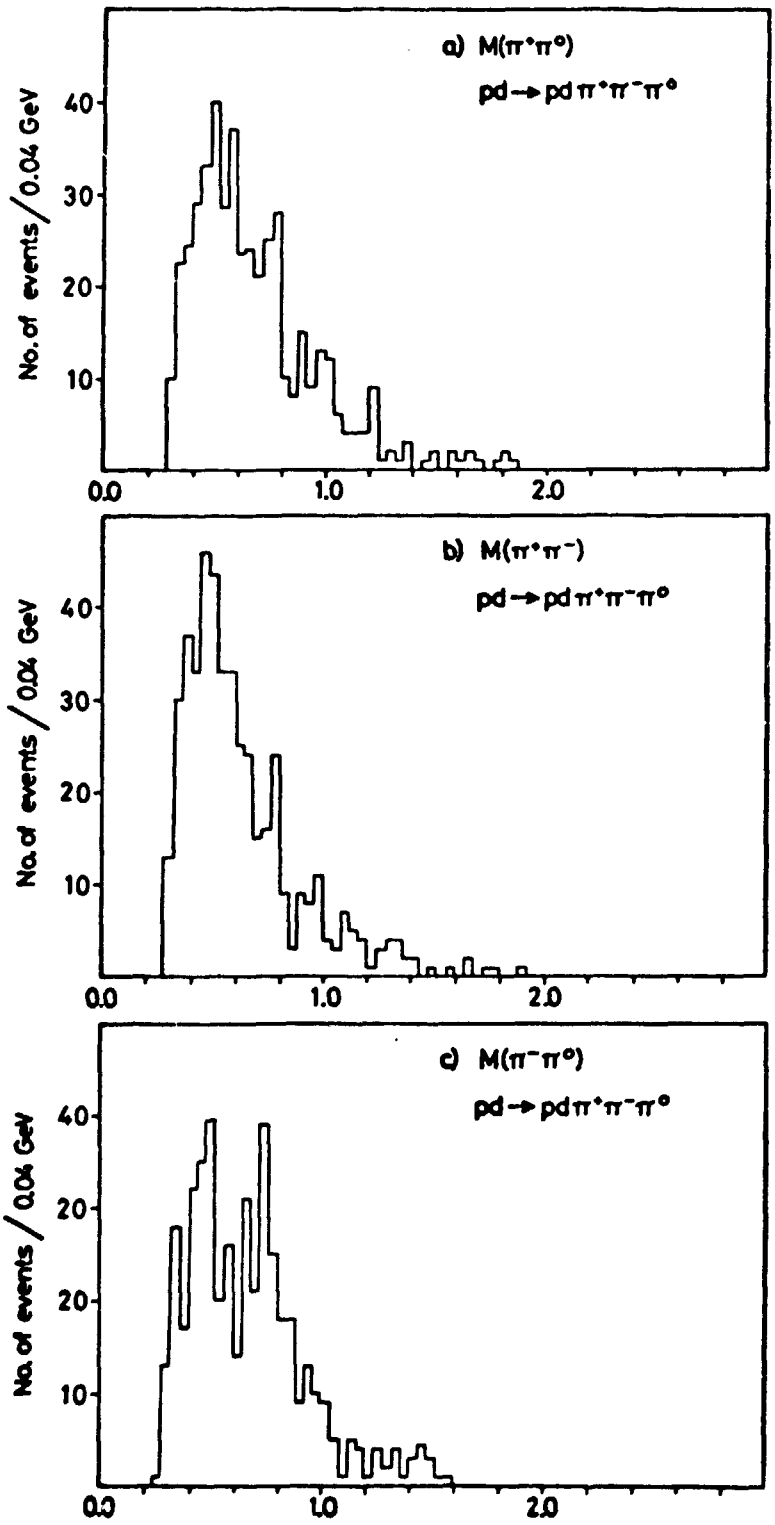
a) M(π⁺π⁰)
pd → pdπ⁺π⁻π⁰
No. of events / 0.04 GeV
40
30
20
10
0.0
1.0
2.0
b) M(π⁺π⁻)
pd → pdπ⁺π⁻π⁰
No. of events / 0.04 GeV
40
30
20
10
0.0
1.0
2.0
c) M(π⁻π⁰)
pd → pdπ⁺π⁻π⁰
No. of events / 0.04 GeV
40
20
20
10
0.0
1.0
2.0

Fig. 6

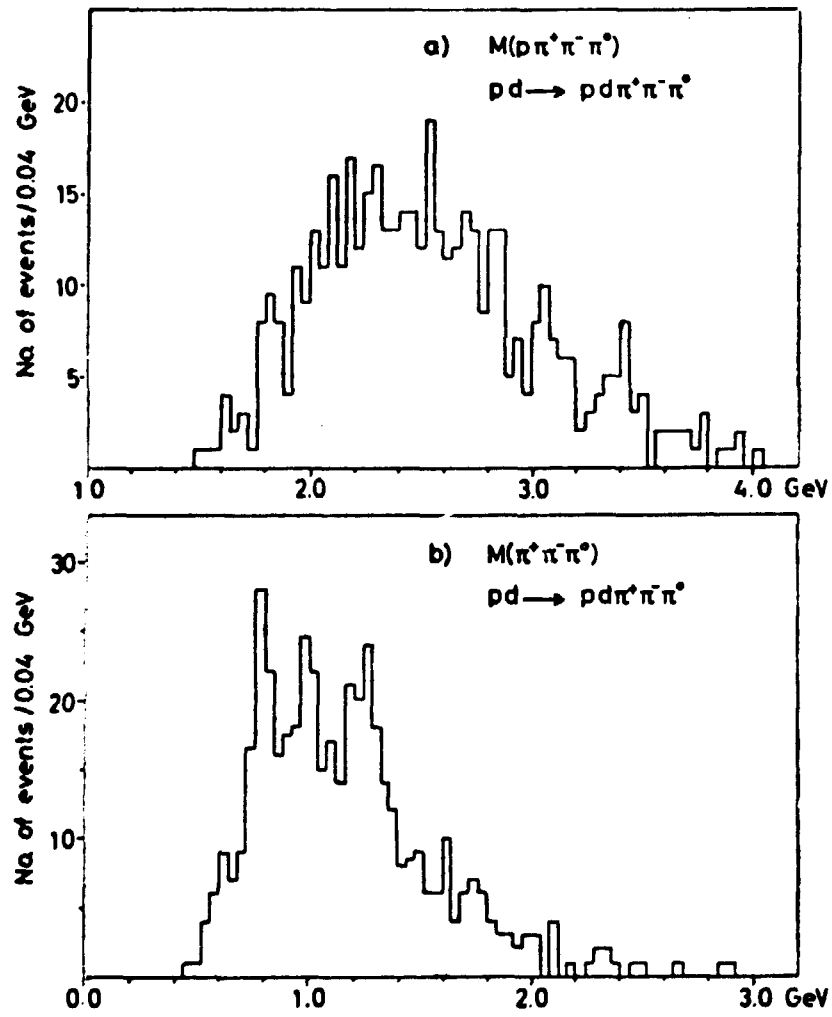
a) M(pπ⁺π⁻π°)
pd⟶ pdπ⁺π⁻π°
No of events/0.04 GeV
20
15
10
5
1.0
2.0
3.0
4.0 GeV
b) M(π⁺π⁻π°)
pd⟶ pdπ⁺π⁻π°
No of events/0.04 GeV
30
20
10
0.0
1.0
2.0
3.0 GeV

Fig. 7

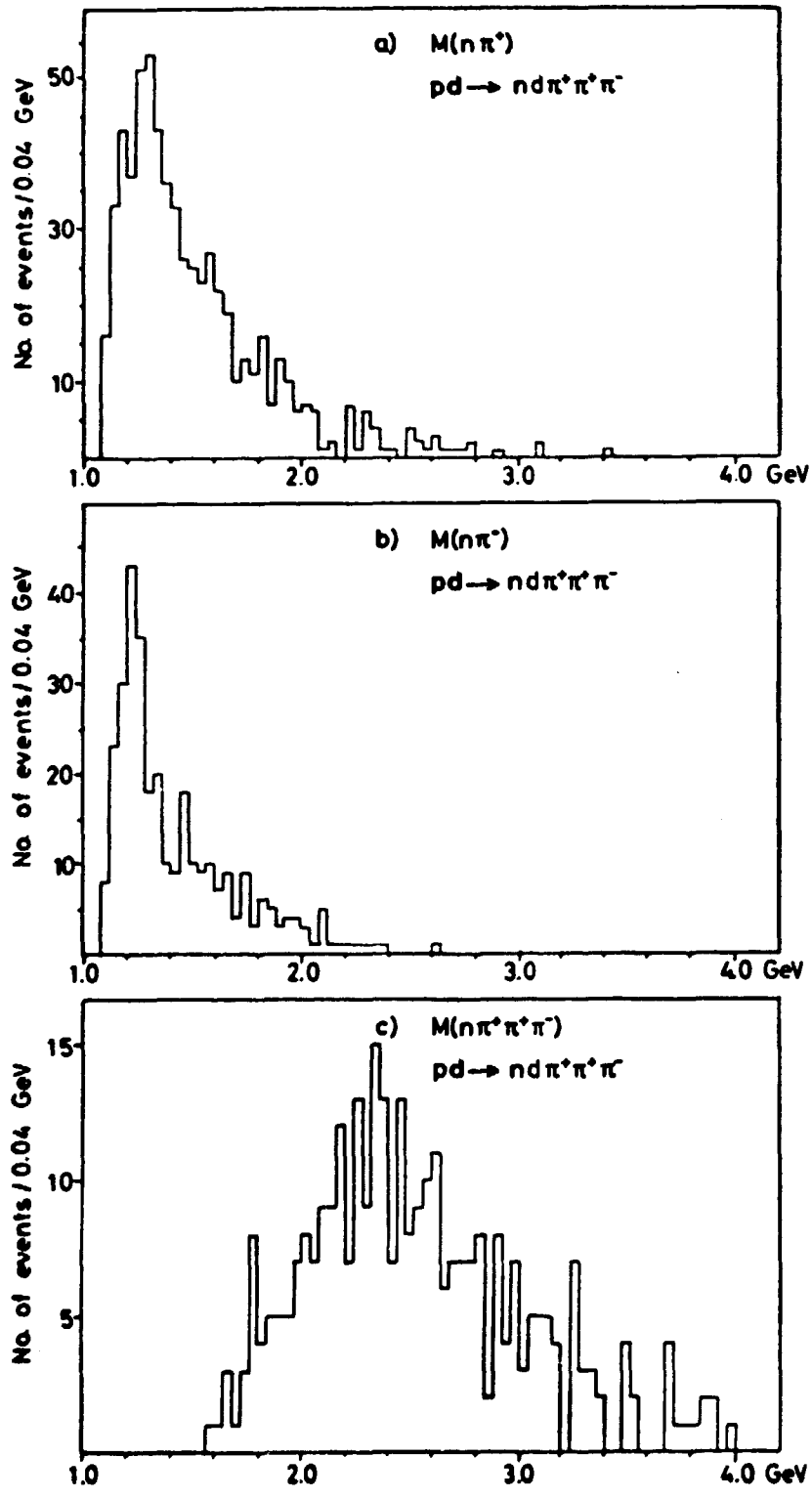
a) M(nπ⁺)
pd → ndπ⁺π⁺π⁻
No. of events/0.04 GeV
50
30
10
1.0
2.0
3.0
4.0 GeV
b) M(nπ⁻)
pd → ndπ⁺π⁺π⁻
No. of events/0.04 GeV
40
30
20
10
1.0
2.0
3.0
4.0 GeV
c) M(nπ⁺π⁺π⁻)
pd → ndπ⁺π⁺π⁻
No. of events/0.04 GeV
15
10
5
1.0
2.0
3.0
4.0 GeV

Fig. 8

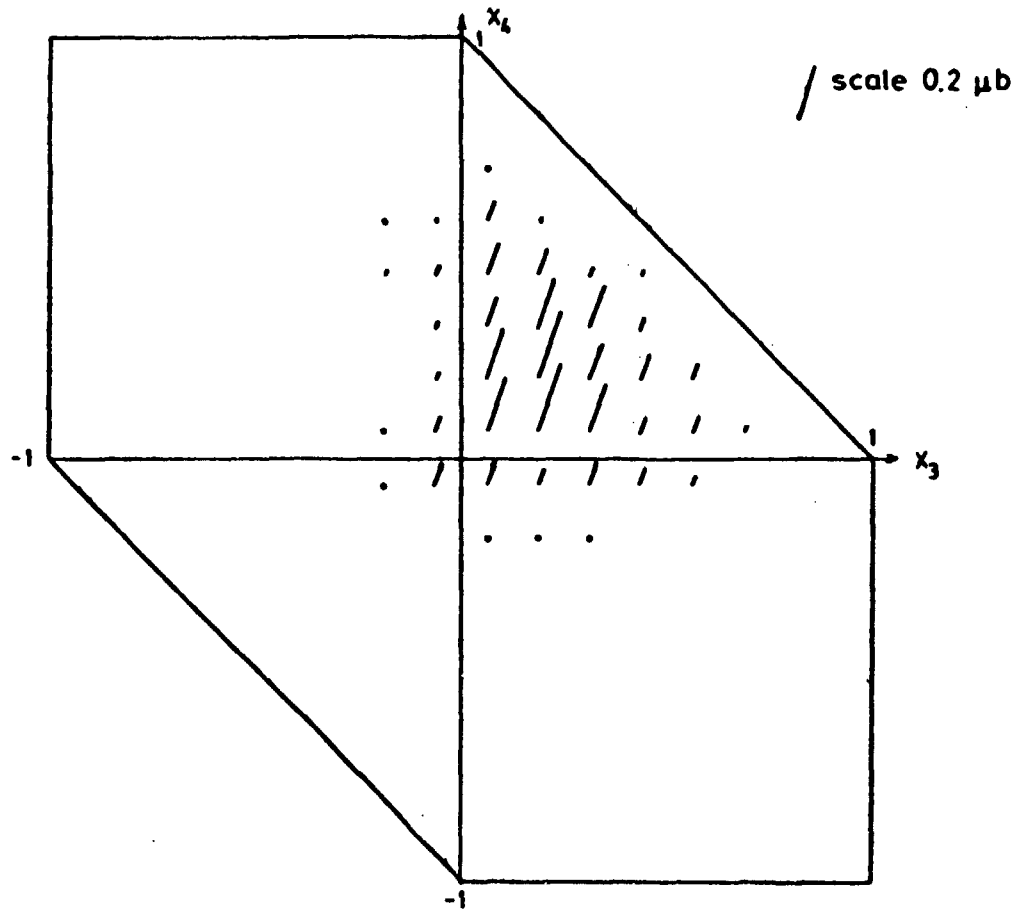

Fig. 9

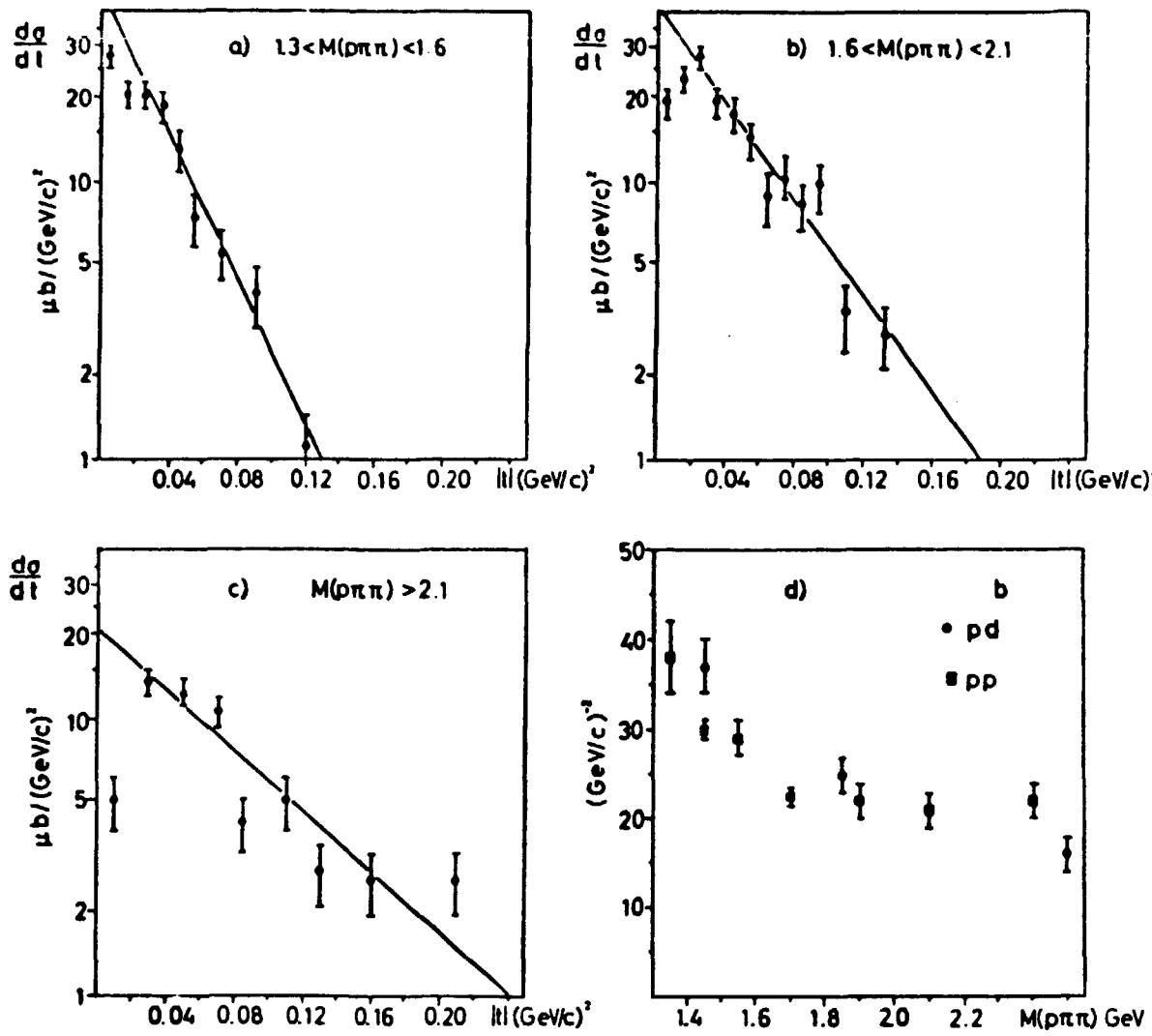
a) 1.3<M(pππ)<1.6
b) 1.6<M(pππ)<2.1
c) M(pππ) >2.1
d) b
pd
pp
dσ/dt
μb/(GeV/c)²
(GeV/c)⁻²
|t| (GeV/c)²
M(pππ) GeV

Fig.10

a)

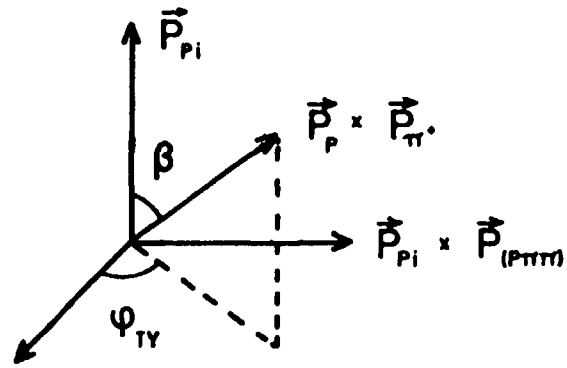
$\vec{P}_{Pi}$
$\vec{P}_{P} \times \vec{P}_{\pi^0}$
β
$\vec{P}_{Pi} \times \vec{P}_{(P\pi\pi\pi)}$
φ_{TY}

b)

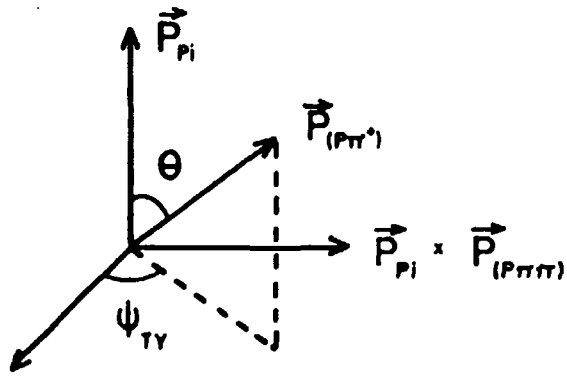
$\vec{P}_{Pi}$
$\vec{P}_{(P\pi^0)}$
θ
$\vec{P}_{Pi} \times \vec{P}_{(P\pi\pi\pi)}$
ψ_{TY}

c)

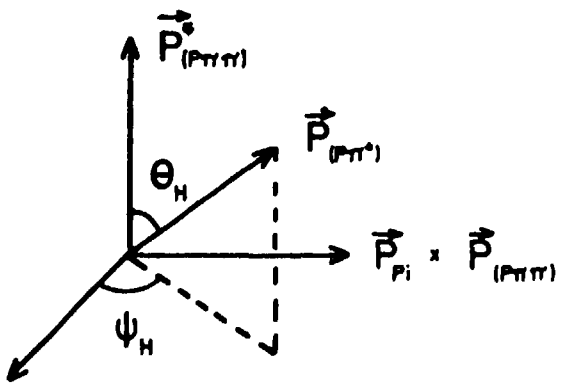
$\vec{P}^{*}_{(P\pi\pi\pi)}$
$\vec{P}_{(P\pi^0)}$
θ_H
$\vec{P}_{Pi} \times \vec{P}_{(P\pi\pi\pi)}$
ψ_H

Fig. 11

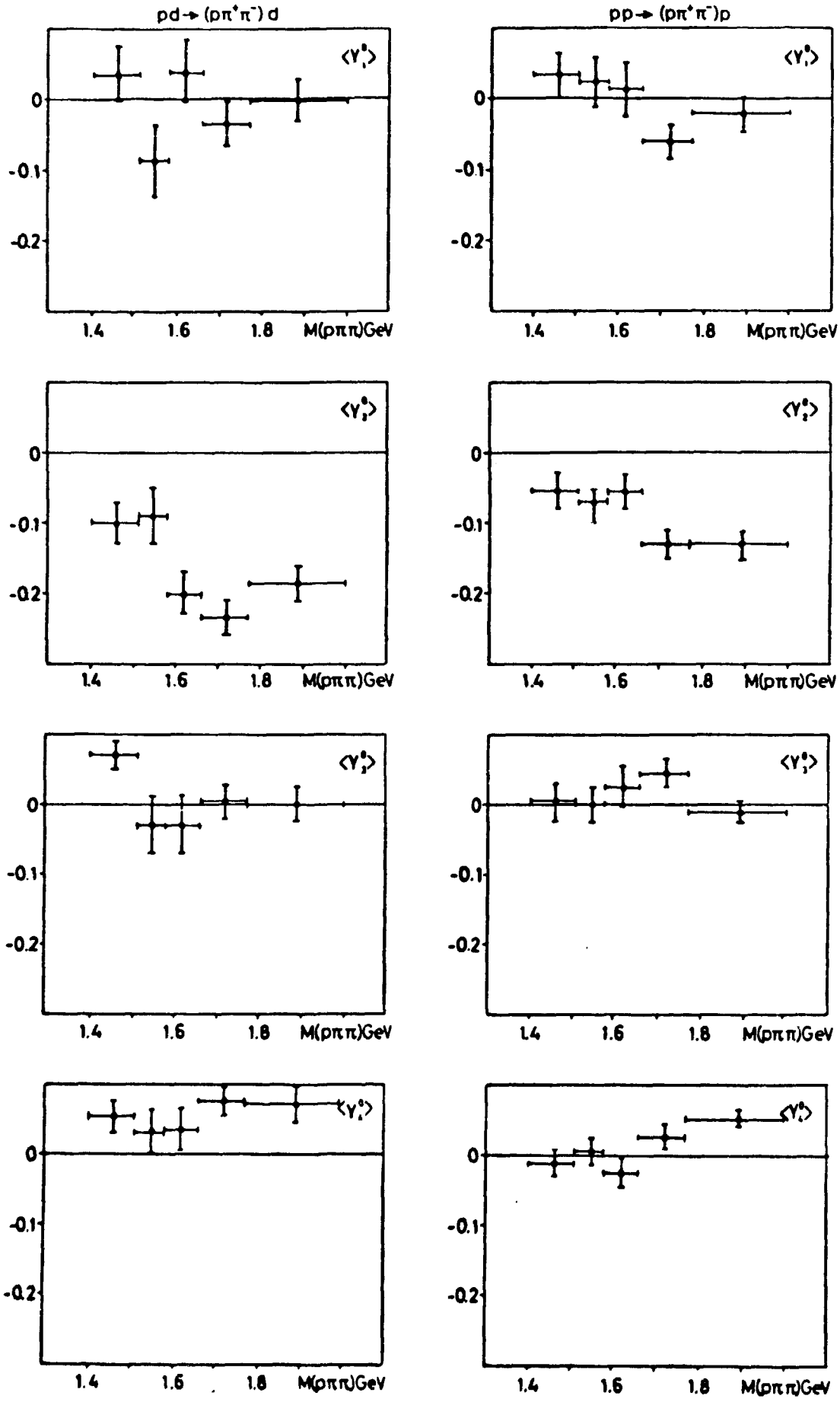

Fig.12

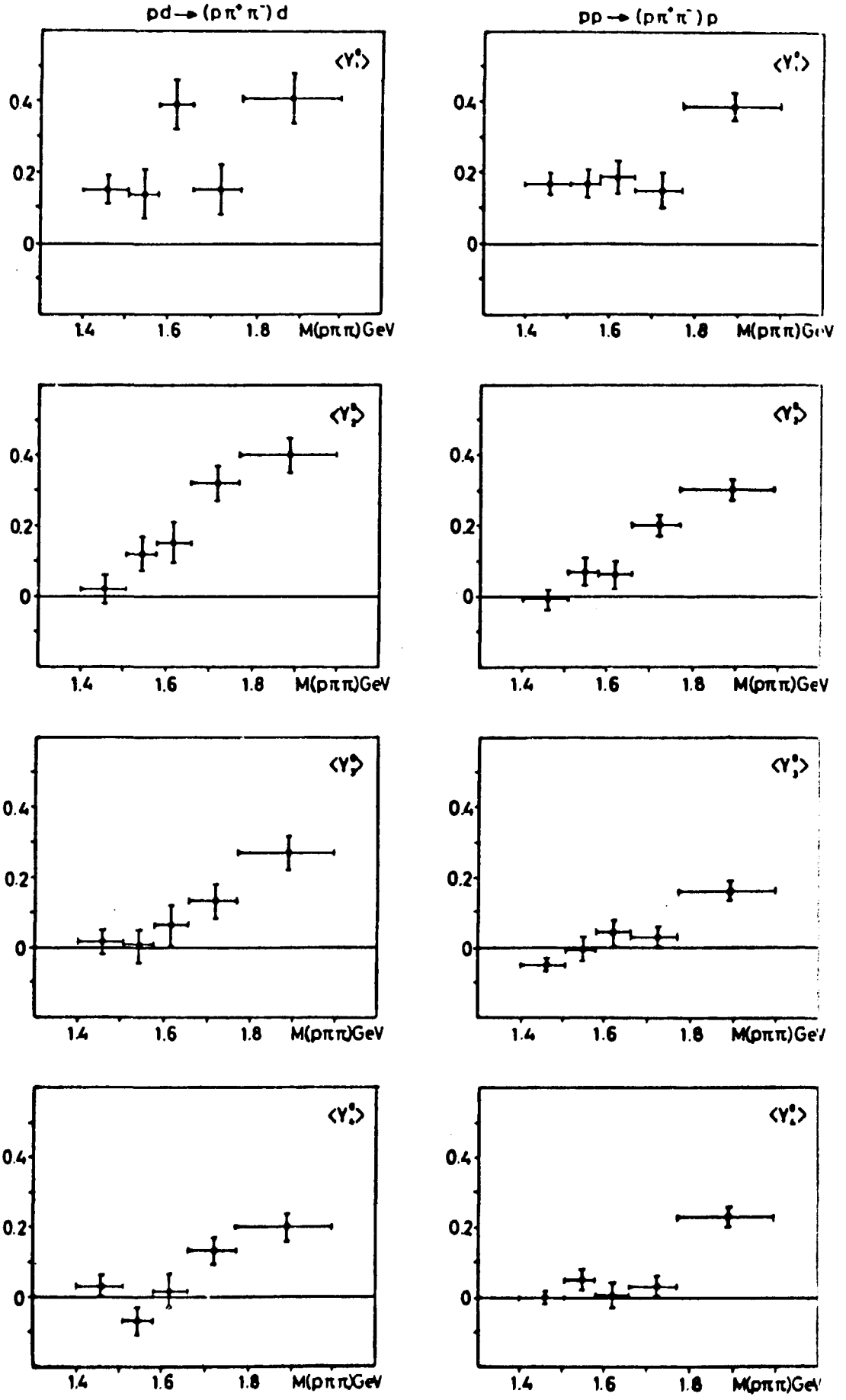

Fig. 13

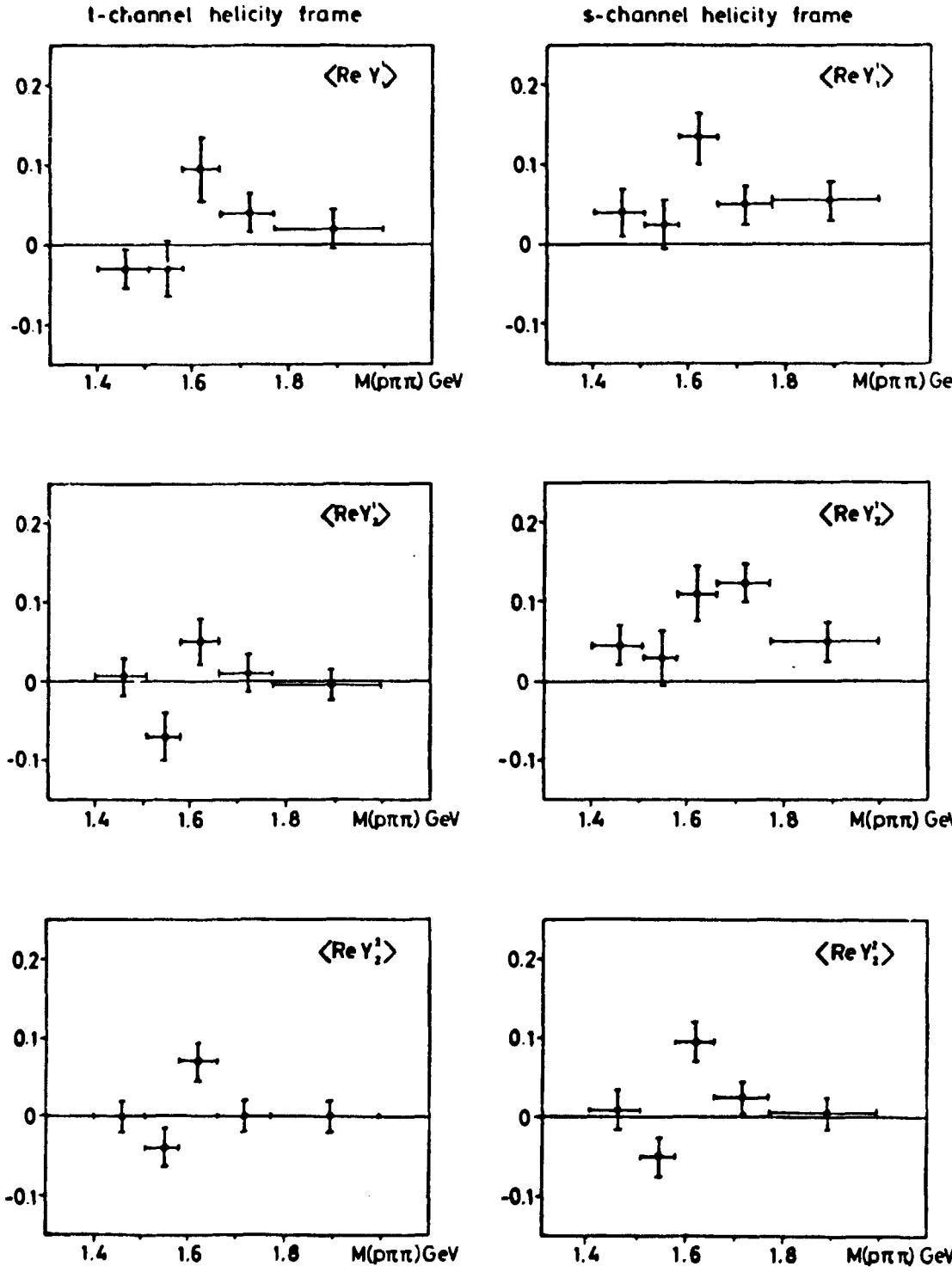
t-channel helicity frame
s-channel helicity frame
⟨Re Y⟩
⟨Re Y'1⟩
⟨ReY'2⟩
⟨Re Y'2⟩
⟨Re Y'2⟩
⟨Re Y'2⟩
0.2
0.1
0
-0.1
1.4
1.6
1.8
M(pππ) GeV

Fig. 14

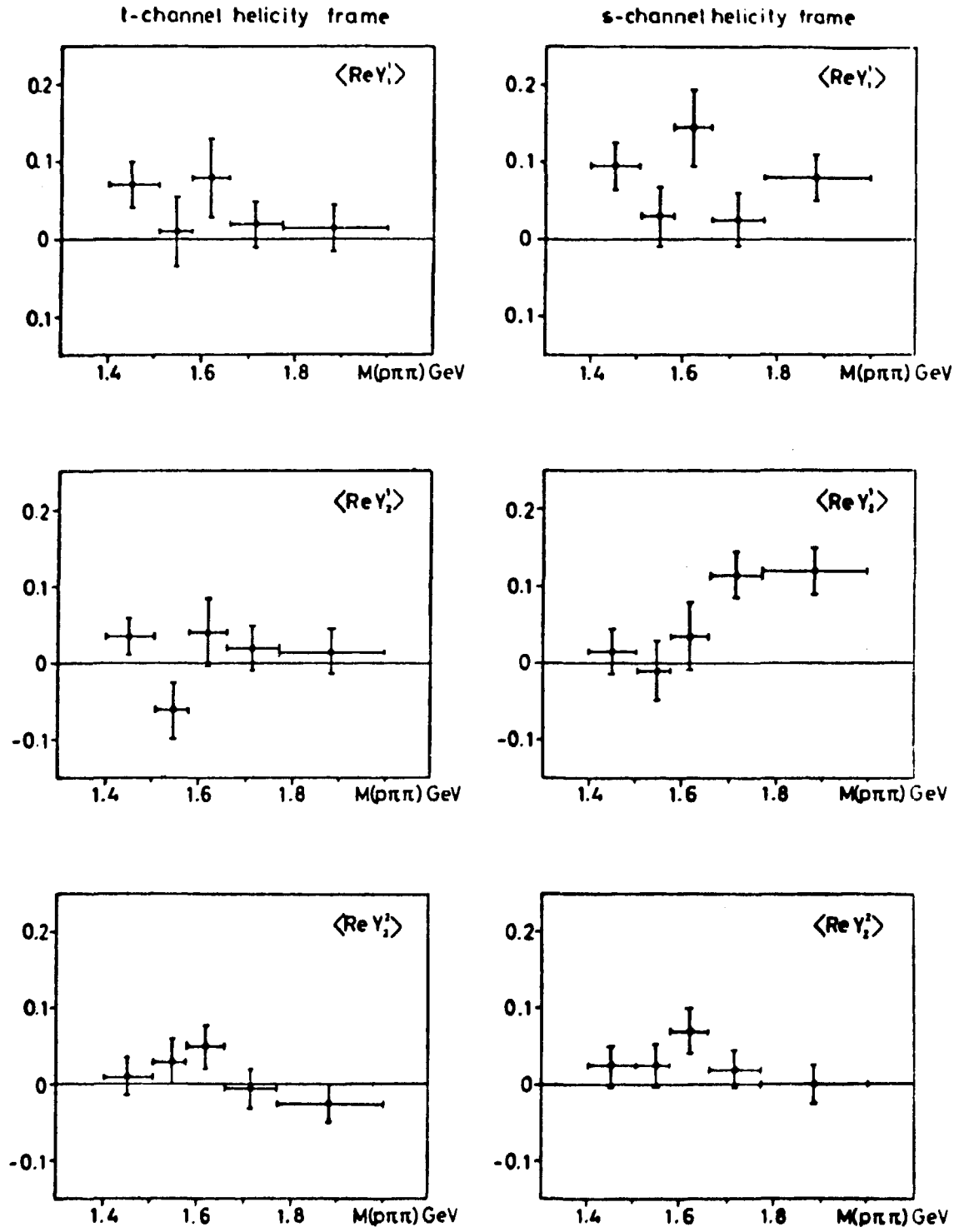
t-channel helicity frame
s-channel helicity frame
⟨ReY'1⟩
⟨ReY'2⟩
⟨ReY'3⟩
⟨ReY'4⟩
0.2
0.1
0
-0.1
1.4
1.6
1.8
M(pππ) GeV

Fig. 15

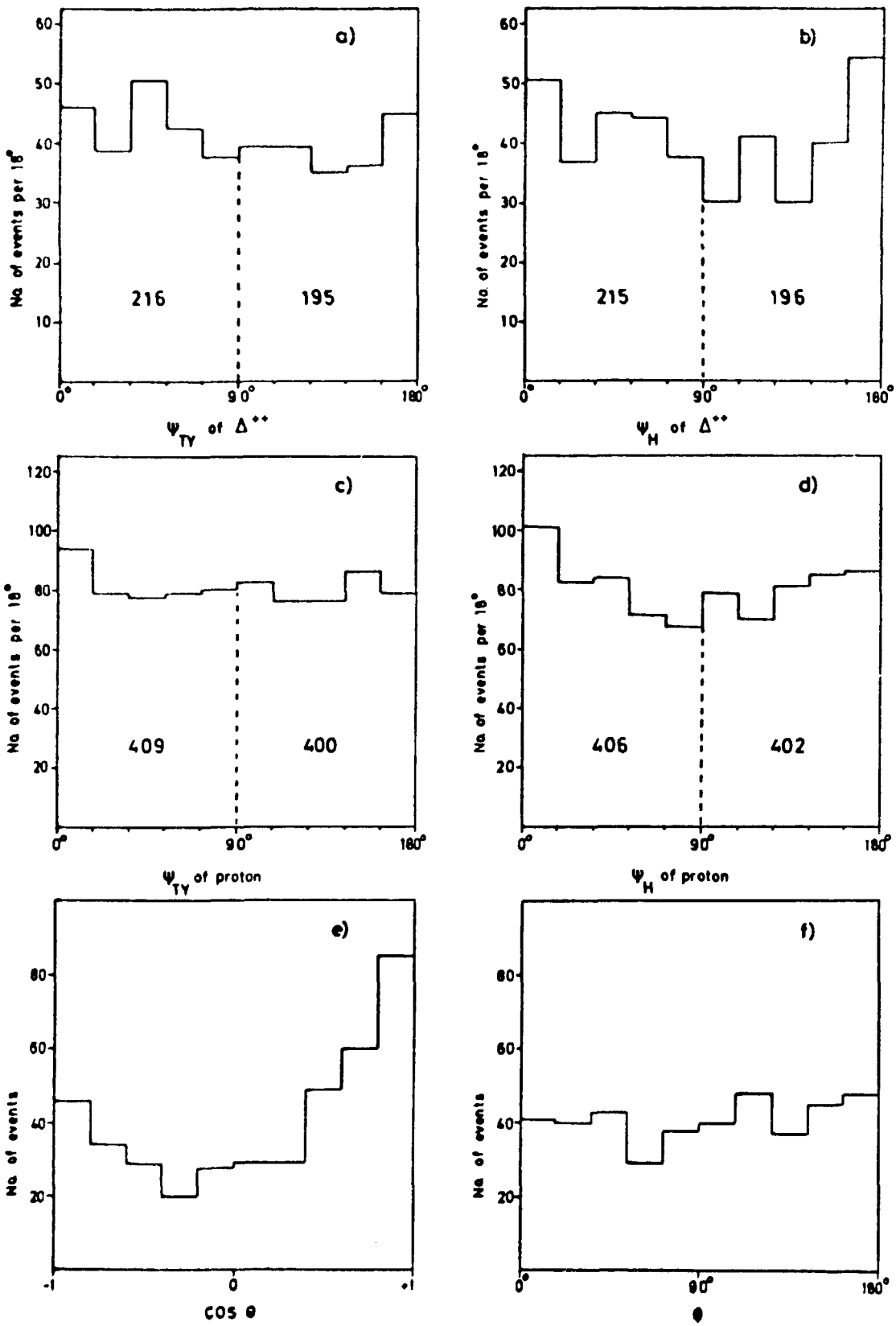
a)
b)
c)
d)
e)
f)
No. of events per 18°
No. of events
216
195
215
196
409
400
406
402
0°
90°
180°
-1
0
+1
Ψ_{TY} of Δ^{++}
Ψ_{H} of Δ^{++}
Ψ_{TY} of proton
Ψ_{H} of proton
cos θ
φ

Fig. 16

UNIVERSITY OF STOCKHOLM
INSTITUTE OF PHYSICS
VANADISVÄGEN 9
S-113 46 STOCKHOLM
SWEDEN